4D imaging and analysis of multicellular tumour spheroid cell migration and invasion

Rosalie Richards[1,*], David Mason[1,*], Raphaël Lévy[1], Rachel Bearon[2], and Violaine Sée[1,✉]

[1]University of Liverpool, Institute of Integrative Biology, Department of Biochemistry; Centre for Cell Imaging, Liverpool, L69 7ZB, UK
[2]University of Liverpool, Department of Mathematical Sciences; Liverpool, L69 7ZI, UK
[*]Contributed equally

Studying and characterising tumour cell migration is critical for a better understanding of disease progression and for assessing drug efficacy. Whilst tumour cell migration occurs fundamentally in 3 spatial dimensions (3D), because of the practicalities of growing 3D cell cultures and the complexities in measuring and tracking movement in 3D over time, most migration studies to date have performed analysis in 2D. Here we imaged live multicellular tumour spheroids with lightsheet fluorescence microscopy to determine cellular migration and invasion in 3D over time (4D). We focused on glioblastoma, which are aggressive brain tumours, where cell invasion into the surrounding normal brain remains a major challenge for clinical management. We developed a workflow for analysing complex 3D cell movement, taking into account migration within the spheroid as well as invasion into the surrounding matrix. This provided metrics that summarize the motion of the cells in different experimental conditions. As a proof of principle, we show how 3D tracking and analysis can be used to evaluate the efficacy of chemotherapeutics on invasion. The rich datasets open avenues for further studies on drug efficacy, microenvironment composition and stiffness, as well as collective cell migration and metastatic potential.

LSFM | SPIM | Lightsheet Microscopy | Cell Tracking | Invasion | Spheroids | Glioblastoma | 3D

Correspondence: ***violaine@liverpool.ac.uk***

PREPRINT

Introduction

The multicellular tumour spheroid is a well-characterised model in which cells are grown as three-dimensional (3D) clusters in the absence of any exogenous support. The spheroid model replicates important aspects of the tumour microenvironment such as gradients in oxygen, nutrients, pH, and cell proliferation and survival (1–3). The cellular and molecular heterogeneity of spheroids makes them a better model for solid tumours than homogeneous monolayer cultures. These pathophysiologically-representative 3D models are increasingly important in cancer research, especially for drug testing. The invasion of tumour cells into neighbouring tissue or distant organs is a hallmark of cancer and a major cause of mortality (4), which urgently needs to be tackled therapeutically. Good *in vitro* models for testing drugs that inhibit cell invasion are therefore essential. The majority of *in vitro* invasion assays to date, and associated drug screening, have been conducted using cells cultured as two-dimensional (2D) monolayers on plastic and glass surfaces (5). These conditions fail to replicate important aspects of the cellular environment that occur *in vivo*, such as complex cell-cell and cell-matrix interactions, matrix stiffness, and gradients in soluble factors such as oxygen, nutrients, growth factors, and cytokines (6). This explains why the results of *in vitro* drug screening often only poorly correlate with results obtained *in vivo*. Hence, drug testing in spheroids is emerging as a beneficial intermediate between testing in monolayer cultures and testing in animals (7). In previous attempts at measuring cellular invasion in 3D models, the spheroids were plated on, or embedded in, extracellular matrix (ECM) in 96-well plates and imaged using an inverted microscope (8–11) providing information about the movement of some of the invading cells (in the x-y plane) but failing to capture the movements of cells within the spheroids. Imaging thick, living samples over long time courses can be challenging due to the effects of light diffraction, photobleaching and phototoxicity (12). Lightsheet fluorescence microscopy (LSFM), also known as single-plane illumination microscopy (SPIM), has overcome some of these challenges. By illuminating only the focal plane of the detection objective, the effects of photobleaching and phototoxicity are much reduced compared to confocal microscopy (13, 14). LSFM also allows for very fast image acquisition from multiple angles, making it the ideal technique for imaging cell movement in a large, tightly packed spheroid, where z-stacks need to be acquired in rapid succession to facilitate the tracking of cells in space. Concurrently, the development of new software tools for spatial-temporal quantification of tumour spheroid dynamics (15) facilitates the analysis of such data rich 3D time lapse experiments. Here we used live LFSM of multicellular tumour spheroids to characterise cellular migration and invasion in 4D. We developed a workflow for analysing complex 3D cell trajectories with either commercial or open source software platform for tracking, taking into account migration within the spheroid as well as invasion into the surrounding extracellular matrix. This generated metrics characteristic of cell motion. These methods are applicable to a range of experimental conditions, including anti-cancer drug treatment. As proof of principle, spheroids were treated with 17-allylamino-17-demthoxygeldanamycin (17AAG), a heat-shock protein 90 (HSP90) inhibitor, and cilengitide, an $\alpha v\beta 3$ and $\alpha v\beta 5$ integrin inhibitor with anti-tumour activity (16). Live LSFM combined with cell motion analysis allowed us to discern the effects of these molecules both on the cells invading away from the spheroid as well as on movement within the spheroid. Both effects may need to be considered

to evaluate the mechanisms and efficacy of anticancer drugs in inhibiting tumour cell infiltration.

Methods

H2B-mRFP-U87MG stable cell line production. A nuclear marker is necessary to facilitate object recognition by the tracking software and enable automated cell tracking. We previously found that nuclear stains with dyes show poor penetration in spheroids, therefore, we created a cell line stably expressing a fluorescent histone H2B nuclear reporter protein by transducing U87-MG cells with pHIV-H2BmRFP. Lentiviral particles were generated by transfecting HEK293T cells with the following plasmids from Addgene (http://www.addgene.org): pHIV-H2BmRFP (Plasmid #18982), psPAX2 (Plasmid #12259) and pMD2.G (Plasmid #12260) in a 4:2:1 ratio. On day 1, HEK 293T cells were seeded in six 10 cm^2 dishes at a density of 1.5 x 10^6 per dish in 10 mL growth media (DMEM + 10% FBS + non-essential amino acids). On day 2, cells were transfected with the aforementioned plasmids using polyethylenimine (PEI) at a ratio of 2 μL: 1 μg PEI:DNA. On day 3, the media was changed and on day 5 supernatant was harvested, centrifuged at 500 x g for 10 min and filtered with a 0.45 μm PES filter before being subjected to ultracentrifugation following the protocol described in (17). 2.5 x 10^5 U87-MG cells were seeded in to a 25 cm^2 tissue culture flask and 250 μL virus was applied. Media was changed after 24 h.

Spheroid culture and preparation. We have previously described a workflow for the growth, handling and imaging of spheroids made with fluorescently-labelled cells (18). The hanging drop method was used to grow compact spheroids from U87-H2BmRFP glioblastoma cells over 3 days (detailed protocol is available in (18)). Three day old spheroids were used to limit the effect of light scattering seen when imaging deeper (past ~150 μm). At the beginning of imaging, spheroids were approximately 300 μm in diameter. Spheroids were prepared for imaging by aspirating the growth media and replacing it with 50% ice-cold Matrigel (Corning, Netherland) and 50% growth media plus 25 mM HEPES. For drug treated spheroids, 0.5 μM 17AAG (Abcam, UK) or 2 μM cilengitide (Adooq Bioscience, CA, USA) was added to the growth media. A Teflon plunger (Zeiss) was used to draw the spheroid into an optically-amenable fluorinated ethylene propylene (FEP) tube (S 1815-04, BOLA, Germany), which was sealed at one end using parafilm, mounted in the Lightsheet Z.1 (Zeiss) sample holder and then immersed in water at 37 °C for the duration of the experiment.

Image acquisition. Samples were excited with a 561 nm laser and 10x excitation objectives; emitted light was collected through a 576–615 band pass filter using a 20x W Plan-Apochromat objective and 1x zoom. Images of the H2B-mRFP-labelled nuclei were acquired every 3 min with a z-step of 1.66 μm, starting approximately 50 μm in front of the spheroid. Lightsheet Z.1 Zen software (Zeiss) was used to acquire images using online dual side fusion with pivot scan. Images were detected using a pco.edge scientific complementary metal–oxide–semiconductor (sCMOS) camera.

Image pre-processing. Processing was done on a high-end workstation (*cf.* a high performance compute cluster), and thus reducing the size of the lightsheet data prior to analysis was essential due to the large file sizes produced (up to 0.75 TB for one experiment). A custom Fiji macro (see code availability below) allowed us to load one time point at a time and to down-sample the data by decreasing bit depth from 16 bit to 8 bit and by performing 2x binning (this is user configurable). A further processing step was carried out in Fiji prior to analyses in order to deal with sample drift (19), using the descriptor-based series registration plugin developed by Preibisch *et al.* (20). Registration was carried out using a translational transformation model and consecutive matching of images with a range for all-to-all matching of two.

Cell tracking. There are many excellent software packages available for tracking points over time (21). In this study, both the commercially-available Imaris 8.2.0 software (Bitplane, Belfast) and the open-source Trackmate (22) were used to produce tracked outputs. The most basic tracking outputs are

1. Position (Cartesian coordinates in X, Y and Z)
2. Time stamp (calibrated time or frame number)
3. Track ID to link features across frames

Although most software provides further analysis such as calculating overall track speed or intensity of spots over time, to give our analysis the widest utility, we wrote our processing scripts to assume no *a priori* track analysis information other than these five outputs. *Imaris* In Imaris, tracking was carried out using an autoregressive motion algorithm, with a maximum distance of 6 μm and a maximum gap size of zero. A filter was applied to remove any tracks that were shorter than eight time points (24 min). Once tracking was complete, the 'Position' spot statistics were exported into a CSV file. *Trackmate* The control datasets were also tracked using the Trackmate plugin (v 3.8.0) for Fiji, using the same parameters as above. The 'Spots in tracks statistics' output of Trackmate were exported into a CSV file. CSV outputs from Imaris or Trackmate can be imported into the MATLAB script for further processing.

Measurement of spheroid boundary and centroid. The spatial location of the outer boundary of each spheroid was defined by taking the mean radial distance of the ten furthest out spots present in the first frame of the experiment and adding 5%. Because part of the analysis relies upon the isotropic nature of a spheroid, the coordinates of the spheroid centroid has to be provided by the user, which allows characterisation of the position and distribution of cells. This is requested from the user at the beginning of the data processing

PREPRINT

script. It is important to use the same software for estimating centroid position as for tracking, as different software may use different frames of reference to define the image origin. Using Imaris, three orthogonal clipping planes were created and positioned centrally to allow the read-out of the relevant position on each axis. The same result can be achieved in Fiji by measuring the X,Y & Z coordinates using the cursor position to read out on the status bar, or alternatively, using the centroid position from a segmented volume.

Analysis of tracking data. MATLAB (Mathworks, US) was used to process the tracking output. A processing script was used to calculate spot and track parameters and a second script was used to create a characteristic set of plots. Briefly, an output CSV file was selected and, when requested, the Cartesian coordinates of the spheroid centroid and the time calibration (sec / frame) were entered. The boundary of the spheroid was calculated as the mean radial distance of the outermost 10 features in the first frame of the movie (see section 8 of the processing script). As spheroid drift was corrected in image pre-processing, this was a reliable measure of the boundary (see Discussion section for commentary on suitability). One of the key functionalities of the processing script is to break apart individual tracks into sections that are within the original spheroid boundary (defined at the start of the experiment) and those outside the boundary. Track-level summary statistics are provided as the mean parameters (e.g. windowed spot speed, windowed straightness, etc.) for all inside and outside sections separately. The proportional time spent inside and outside can be inferred.

Plotting and visualisation. The main output of the processing script is a MATLAB workspace (.mat) file containing all of the calculated values for the features and tracks (see the code repository for a detailed description of the output tables). For meaningful visualisation, a second script was created, providing the summary plots shown in the figures. The plotting and output options of this script are controlled by a number of variables whose parameter space and functions are detailed in the script header (for example axis line widths, font sizes, etc). Other than the input and initialisation code section, each plot is written as a MATLAB section allowing the code to be run in completion or in sections to output only the desired figures. We have found Zegami (`http://zegami.com`) to be a useful tool for querying and investigating the large number of graphs that are produced by the script processing. The output supporting the datasets in this study are openly available and can be explored at `http://zegami.liv.ac.uk` under the project "Spheroid Tracking Data".

Code Availability. The pre-processing Fiji script and the processing and visualisation MATLAB scripts are available at `https://bitbucket.org/davemason/lsfm_scripts` along with documentation and example tracking data. At time of publication the commit hash is `95a4329`.

Results

Single track analysis in 3 dimensions. Previous attempts to describe the migration of spheroid-associated cells over time have largely focussed on gross morphological changes to the spheroid itself, using 2D imaging or 3D projections (23). Such depictions may miss important dynamics occurring at a single cell level or within the body of the spheroid. This is shown in Figure 1A, where a 2D (maximum intensity) projection of two time points is displayed. To characterise single-cell movement, we developed an analysis pipeline to quantify the migration of single cells through post-acquisition tracking and track analysis (see overlaid tracks in Figure 1A). In this experiment, we observed cell migration within the spheroid as well as invasion into the extracellular matrix (Supplemental Movie 1). We tracked cell movements and obtained tracks from 3 control spheroids. One such track, showing the movement of a single cell, is shown in Figure 1B. Yet, the challenge is to extract parameters that allow to capture the behaviour of the population of cells as a whole, in particular in the context of invasion. It is therefore critical to assess the distribution of single track or single spot data. We found both the speed (Figure 1C) and straightness (Figure 1D) to be informative statistics for describing the motion of cells within and outside the spheroid. Unlike track analysis in an embryo (24) or tissue, spheroids are isotropic. With a defined centroid, a boundary can be demarcated between the edge of the spheroid and the surrounding matrix (see Methods) and thus all tracks have a geometric frame of reference (Figure 1E). Therefore, the track positions can be characterised by their radial distances, and sorted into two categories depending upon whether they remain within the spheroid boundary or cross the boundary and invade the surrounding matrix (see Figure 1F).

Cell Population Analysis . One of the most basic features of metastatic cancer cells is invasion; i.e. their ability to leave their initial niche and migrate elsewhere within the close microenvironment. However, there is no clear metric to define and characterise invasion and the extent of invasion is often underestimated through the projection of a 3D+time experiment onto 2D+time either through the imaging (for example imaging a single z-plane) or post-acquisition using a projection in the z-axis. By locating cell nuclei, we captured an accurate picture of invasion into the surrounding matrix and represented this through a cumulative distribution plot (Figure 2A). This type of plot describes the location of the cells at the start of the experiment (blue line shows frame 1) and how the distribution of the cells radial positions changes over the course of the experiment. Compared to a 2D projection, one important advantage is that information in the z-plane is preserved. Two interesting insights are gleaned from this plot. Firstly, the increase in the plateau (Figure 2A) in the raw data plots, suggesting an increased number of features being located at later time points, for example as a result of cell division. Secondly, if the plots are normalised (Figure 2B), the shift of the curve to the right and indeed the shape of the

PREPRINT

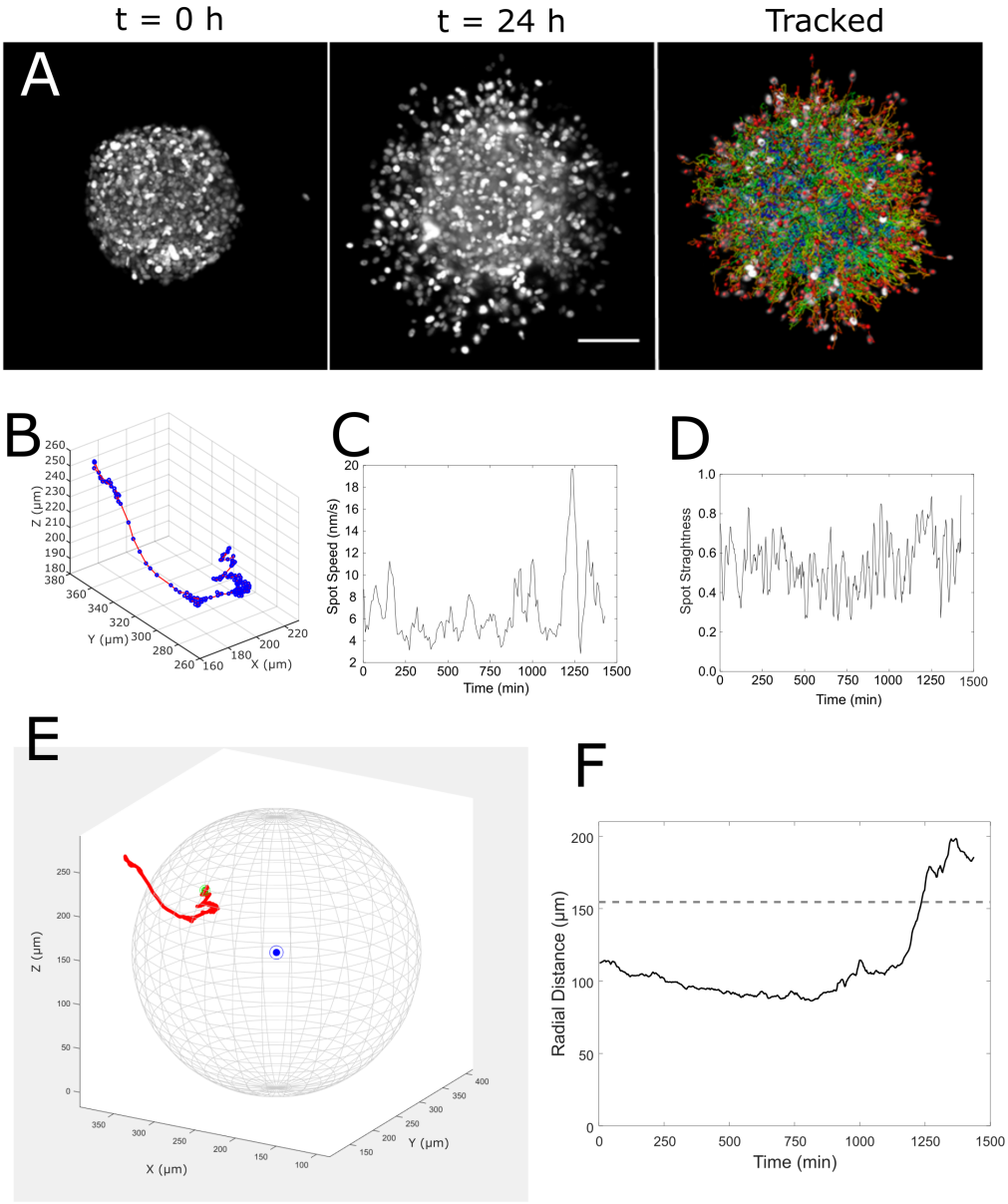

Figure 1. Single Trajectory Analysis. Glioblastoma spheroids made with U87MG cells expressing H2B-mRFP were grown for 3 days, mounted on a lightsheet microscope (t=0 h) and imaged for up to 24 h. (**A**) Maximum intensity projections. Invasion of individual cells can be tracked as they invade the surrounding matrix (tracking is done on full 4D datasets). (**B**) Cell tracking with single-track-level information. (**C**) Instantaneous speed and (**D**) straightness plotted over time. Straightness was calculated in a five frame window by dividing the end to end displacement over five frames by the sum of the displacements along the path length. This time-windowed approach (typically 5 frames ~12 minutes) was necessary to smooth the data while retaining good granularity (**E**) The position of the track from its start point (green dot) in relation to the boundary can be visualised, given the coordinates of the spheroid centroid (blue dot). (**F**) The radial distance is used to follow migratory events (dashed line represents the spheroid boundary).

curve itself, indicates changes in the distribution of the cells over time. Looking at the curve shape may indicate whether cells are primarily moving from the edges of the spheroid into the matrix or whether there is an expansion across the whole spheroid. For the dataset shown, a possible interpretation is an initial invasion largely from the cells within ~30 μm of the surface (Figure 2B: compare 0 h and 8 h) followed by a later expansion of the whole spheroid (Figure 2B: compare 0 h line and 16 h). The cumulative distribution of features effectively ignores the movement of cells in favour of their position at a given time; however, the tracking data are incorporated in the analysis and thus the distributions of speed and straightness parameters can be studied both as a function of radial distance (Figure 2C, D) and as a function of time (Figure 2E, F). We can show, for example, a mean track speed (± standard deviation) of 27 ± 10 μm/h within the spheroid boundary (blue line Figure 2C) and 29 ± 12 μm/h in the surrounding matrix. Being able to query the data in this way is useful because many perturbations in migration, induced for example by a drug treatment or genetic manipulation, may have an effect as a function of distance (a possible proxy for cell density, cell-cell contacts, effector molecule concentration gradient, etc.)

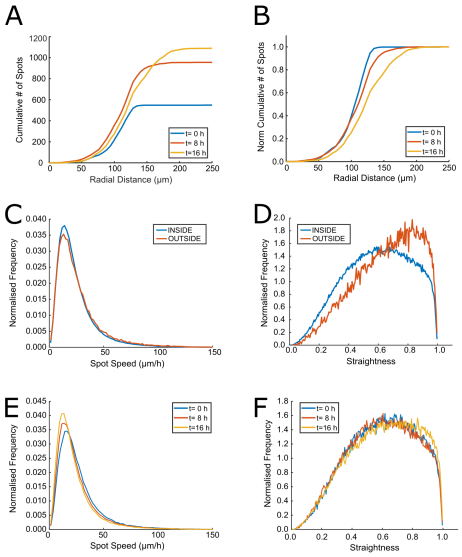

Figure 2. Population Level Analysis. (**A**) The cumulative distribution of detected nuclei by radial distance from the centroid is shown at three different time-points for a control spheroid. (**B**) The graph shown in (A) can be Y-axis normalised to better study the changing shape of the distribution. (**C** & **E**) Distribution of spot speeds and (**D** & **F**) straightness. Data shown as a function of radial distance (**C** & **D**) in two bins; inside (blue line; in this spheroid, a radial distance of 0-170 μm) and outside (orange line; a radial distance greater than 170 μm). Data shown as a function of experiment time (**E** & **F**) in three bins each representing the following 8 hours. The plots are normalised to equal area.

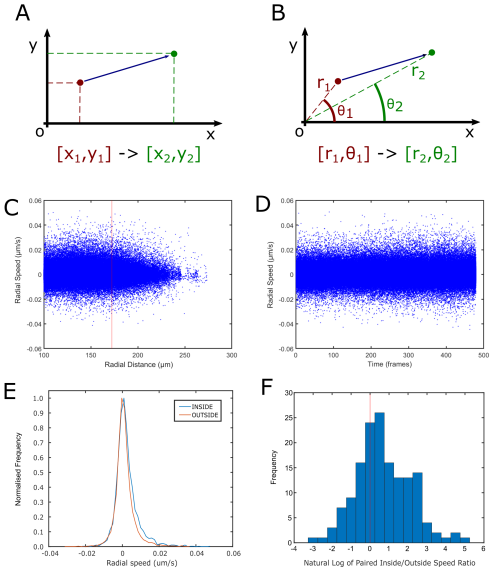

Figure 3. Analysis of radial components The isotropic nature of a spheroid makes it well suited to a spherical coordinate system over Cartesian. (**A**) A 2D example of a Cartesian coordinate system and (**B**) of a circular coordinate system, which extends into 3D with the addition of "z" and ϕ (phi) axes respectively. Radial velocity vectors are calculated and describe the movement in to (negative value) or out of (positive value) the spheroid. This can be investigated as a function of distance from the spheroid centroid (**C**) or time of the experiment (**D**). The red vertical line in (**C**) represents the calculated spheroid boundary (see Methods). Within the context of the spheroid boundary, the radial velocity vectors also allow interrogation of the difference in radial velocity (**E**) when moving within the spheroid (**E**: Inside) or in the surrounding matrix (**E**: Outside). Although not all cells leave the spheroid boundary, for cells that migrate (either way), the paired ratio (inside/outside parts of the same track) can be calculated to show relative changes in the radial velocity. The distribution of the natural log of the ratios is shown (**F**) where zero (red vertical line) represents no difference inside and out, and a positive skew indicates slower speed inside. Panel (**F**) includes the results from three control experiments.

or time (which may be relevant to the sensitivity of feedback loops or cell cycle dependence). In this model, distance is especially relevant given the composition and physical properties of the embedding gel. The normalised plots in Figure 2C, D are shown with two bins of spatial data corresponding to inside vs outside (based on the initial size of the spheroid – see details in Methods). They demonstrate that while there is no discernible difference in speed, the straightness is increased outside the spheroid boundary. The number of spatial bins are configurable by the user if, for example, when using a larger spheroid a greater number of bins would be more appropriate (see Methods section: Plotting and visualisation).

Analysis of radial components and track breakdown. As spheroids are spatially isotropic systems, the movement of cells is best described in spherical coordinates in relation to the centre of the spheroid. Velocity vectors can then be calculated for azimuthal, elevational and radial components (Figure 3A, B show examples of the different coordinate systems for a 2-dimensional system). The radial velocity was plotted as a function of the distance from the centre of the spheroid (Figure 3C) or as a function of time (Figure 3D). In the spheroid model, the sum of positive (i.e. outward) and negative (i.e. inward) velocities, tend to approximate zero. We wanted to investigate if the migration patterns were different for cells migrating within the spheroids or cells invading into the extra-spheroid space (or migrating back into the spheroid). The 'migratory' tracks (i.e. those which cross the boundary in either direction) into their inside and outside components were separated, taking into account multiple transitions. This allowed the comparison of all of the inside and outside components within an individual track. Despite the relatively few cells that migrate into the surrounding matrix over the course of the experiment (~15% of total number of cells detected), a slight positive skew can still be seen when the distribution of radial velocities is plotted separately for vectors inside and those outside the spheroid boundary (Figure 3E). Furthermore, by pairing the components of single tracks, it is possible to get a clearer picture of whether individual cells behave differently in the matrix compared to within the spheroid. The distribution of the natural log of the paired ratios are plotted in Figure 3F. The data are presented this way such that zero (shown with a red vertical line) represents no difference when comparing inside versus outside speeds. The positively-skewed data (with mean of the absolute values being 6.6) indicate the absolute radial velocity of cells decreases when migrating through the matrix compared with their time inside the spheroid.

Testing anticancer drugs effects on cell migration and invasion. To assess the suitability of this 3D single cell-tracking approach as a method to evaluate inhibitors of invasion, we treated spheroids with 17-allylamino-17-demethoxygeldanamycin (17AAG) and cilengitide. Both drugs were added to the cell culture media during sample

PREPRINT

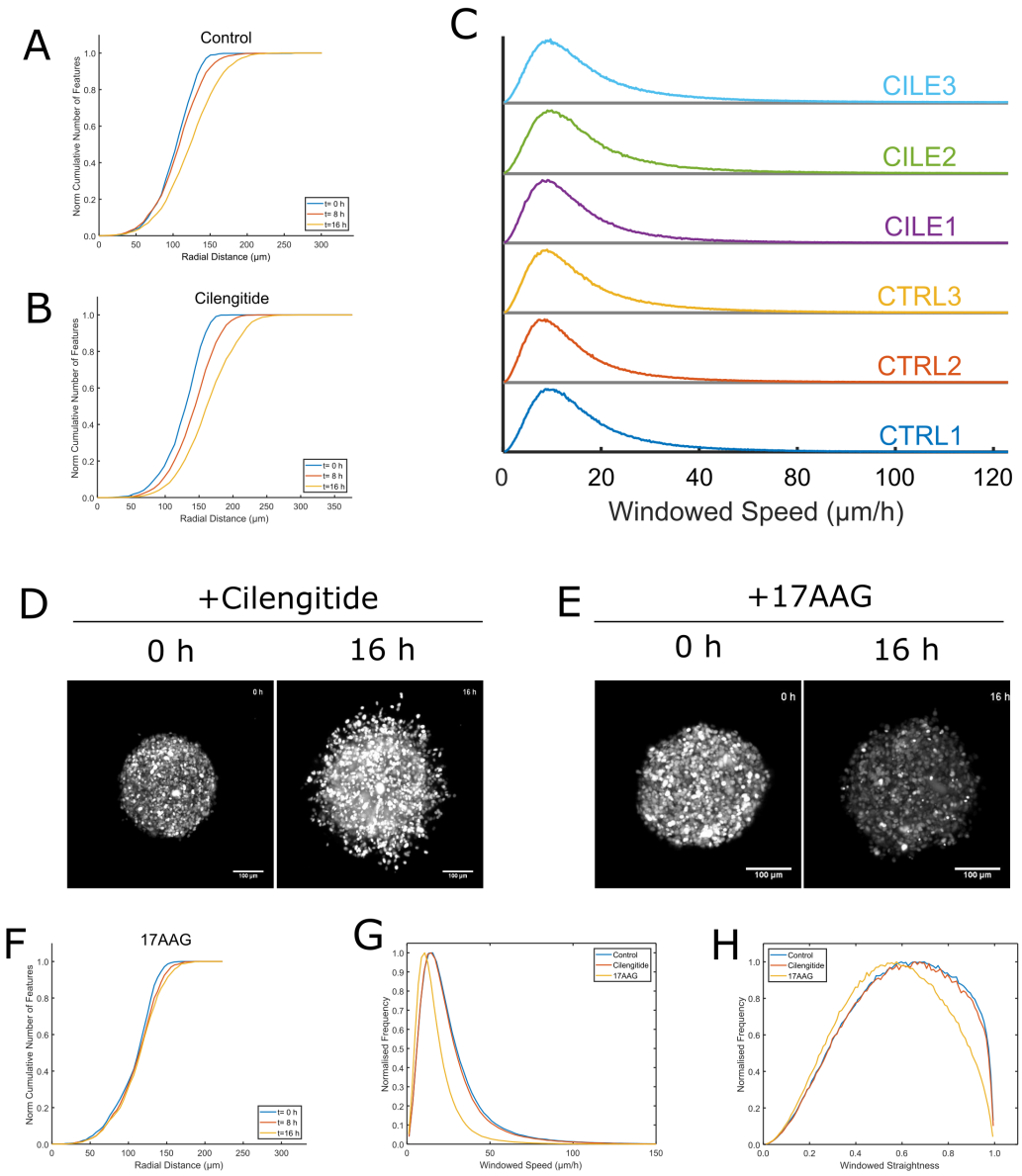

Figure 4. Perturbing migration with chemotherapeutics. The cumulative distribution of cells (as a function of distance from the spheroid centroid) in control (**A**) and cilengitide-treated (**B**) spheroids over time. (**C**) Distribution of windowed speed. (**D**) Maximum intensity projection for comparison of cilengitide spheroids with untreated control spheroids (see Figure 1A for comparison) at 16 h. (**E**) Maximum intensity projection of 17AAG-treated spheroids invasion across the experimental time course. The cumulative distribution of cells (as a function of distance from the spheroid centroid) in 17AAG-treated spheroids (**F**) over time. (**G**) Distribution of the mean windowed speed. (**H**) Distribution of mean windowed straightness. Panels (**G**) and (**H**) include the results from three experiments per condition.

embedding in Matrigel. 17AAG has been shown to inhibit the growth and invasion of glioma cells by inhibiting heat shock protein 90 (HSP90), a chaperone protein that regulates numerous signalling proteins, including those involved in cell proliferation, survival, migration and invasion (25–27). Cilengitide is a cyclic peptide antagonist of integrins $\alpha V\beta 3$ and $\alpha V\beta 5$ that has recently been in clinical trials for recurrent and newly diagnosed glioblastoma (28). The evidence of the effect of cilengitide on invasion is mixed: while some reports document an anti-invasive effect (29, 30), others have found that it acts to promote cell detachment, migration and invasion in 2D cell-based assays (31). Similar to Maurer *et al*, we observed that cells treated with cilengitide showed more rounding up, presumably due to the impairment of adhesion properties (Supplemental Figure 1A). To clarify the role of integrins in the different steps involved in invasion, we initially tested the effects of cilengitide on 2D cell migration. Cilengitide slightly increased the distribution of mean track speeds compared to untreated controls and triggered cell detachment from the cell culture dish (Supplemental Figure 1B). However, when 3-day spheroids were treated with the same concentration of cilengitide, invasion into the matrix was not inhibited (Figure 4A, B and Supplemental Figure 2). The distribution of the windowed speed was comparable between control and cilengitide treated conditions (Figure 4C and Supplemental Movie 2). The absence of cilengitide effects in the 3D model conflicts with the detachment and changes in migration observed in 2D cell cul-

ture, and demonstrates the risks of extrapolating results observed in simple models to more complex ones, as the integrin composition is likely to change (32) (see discussion). Conversely, upon HSP90 inhibition with 17AAG, a lack of invasion was immediately evident from the time-lapse (compare Figure 4D to 4E after 16h and Supplemental Movie 3). The cumulative distribution graph (Figure 4F and Supplemental Figure 2) was also markedly different than the control (Figure 4A) and the cilengitide treated spheroids (Figure 4B) with only a small amount of curve shift at the very edge of the spheroid. Furthermore, the distributions of both the speed (Figure 4G) and straightness (Figure 4H) of the 17AAG-treated spheroids were decreased compared to control and cilengitide treated, suggesting both slower and more tortuous motion. In summary, we have developed a workflow for the analysis of spheroid cell migration and invasion data. The acquisition, post-processing and parameter extraction of single cell movement in spheroids allows effects of chemotherapeutic drugs on cell migration and invasion to be tested.

Discussion

While spheroids have previously been used to investigate invasion, these investigations have until recently been limited by the available imaging techniques and a lack of clear metrics by which to quantify and compare conditions. Projecting 3D imaging data or relying on 2D imaging alone can make the processing and analysis easier, yet this inherently decreases the accuracy of the measurements. We described here a workflow to aid in the acquisition and analysis of 4D data from lightsheet imaging, using spheroids derived from glioblastoma cells as a model system. By imaging and tracking individual cells, we were able to gain many of the broad insights provided in 2D acquisition systems as well as leveraging the detailed information gleaned from the 3D nature of the system.

3D cell microenvironment and migration speed. In line with *in vivo* observations, we recorded a high mobility of cells within gliobastoma spheroids. Under control conditions, the mean track speed of 27 μm/h within the spheroid boundary, correlates well with the results of Farin *et al* in which glioma cells injected into neonatal rat forebrains were tracked and evaluated to move at 25 μm/h in sectioned tissues when imaged (as with our experiments) every 3 minutes (33). However, the tissue microenvironment and its properties are likely to affect cell migration. Indeed, we found that track straightness was consistently increased in cells that were invading into the Matrigel compared with cells that were migrating within the spheroid (Figure 2D). It has been previously described how the speed and mode of cellular invasion are modulated by properties of the ECM such as composition, matrix stiffness and pore size (34–37). Our experimental and analytical workflow provides a precise and quantitative measurement of the cell migration properties that can be used to assess these changes. One question that remains unanswered is whether cells migrating out from a spheroid are creating new pores, or using existing holes created by cells that have previously left. With slight adaptations such as using fluorescently labelled matrix or cell body (see below), this workflow can be adapted to study this type of cell migration. Nevertheless, there are several advantages to nuclear tracking, chiefly that feature detection and segmentation during tracking is considerably more robust especially if cells are in contact. Touching cells expressing a soluble GFP or other cytosolic or membrane label are harder to segment within a complex 3D structure. Moreover, nuclear tracking allows the possibility of gathering additional information on cell division if required.

Drug effects on cell invasion versus cell migration. To compare cell motion into the surrounding matrix to movement within the spheroid, a boundary has to be defined. The position of the boundary is somewhat arbitrary because there is a continuous transition in cell density between inside and outside of the spheroid. Here we opted for a simple definition of "inside" and "outside" based on the initial time point. We found this to be a robust and useful functional definition and furthermore can be used to reliably segment tracks as the "core" of the spheroid does not appreciably change in size during the experiment. Of note, the open availability of the code makes it simple for others to adapt the boundary calculation or indeed any other part of the data processing. Our results show that 17AAG prevented the invasion of cells into the Matrigel but interestingly did not prevent their migration within the spheroid, although the movement of cells inside 17AAG treated spheroids was slower and less directional than in control spheroids. 17AAG affects many signalling proteins through its inhibition of HSP90, making it difficult to pinpoint the mechanism through which invasion is inhibited (25, 26, 38). However, it has been shown that treatment with 17AAG and HSP90 inhibition modulates actin dynamics, thereby affecting cell migration and invasion (39). In contrast to 17AAG, we found that cilengitide was not effective in inhibiting invasion and, furthermore, we could not detect any differences between spheroids treated with cilengitide and control spheroids. Cilengitide reduces cell viability by causing cell detachment (anoikis). The sensitivity of U87 cells to cilengitide-induced detachment has been shown to be dependent on the composition of the ECM, with cells cultured on collagen-coated plates resisting detachment (31, 40). Gritsenko and Friedl have recently demonstrated that β_1 and α_v integrins represent the primary adhesion systems for glioma cell migration in different migration models (spheroids and organotypic brain slices) (32). However, when they compared the same integrin interference strategy in the different models, they observed a variation in the contribution of integrin-dependent glioma invasion. Their results suggest that there are alternative cell-matrix interactions in complex brain-like models, which drive different cell migration properties and require specific inhibitors. This illustrates the importance of replicating environmental factors, such as ECM composition, to obtain a valid assessment of

PREPRINT

anti-invasive or anti-tumour activity and points to the fact that even more complex models than single cell type spheroids might be necessary for *in vitro* drug testing. Nevertheless, the accurate measurement of cell velocity and movement, highly comparable to previous studies using glioma cells by Farin *et al* (33), supports the use of live spheroid imaging in drug screening, prior to costly investigations in preclinical animal models. Moreover, our approach has overcome some of the limitations faced by Farin *et al*, who were only able to track the movements of cells in the x-y plane (33). In conclusion, light sheet microscopy provides an excellent method for measuring cellular movements in multicellular tumour spheroids, providing not only high quality time-lapse images but also a framework to track and analyse these dense structures. Our findings with the two anti-cancer drugs tested indicate that it also holds promise for screening and investigating the mechanism of anti-invasive drugs, contributing to the principles of the replacement and reduction of the use of animals in experimental research.

ACKNOWLEDGEMENTS

The microscopes used for this work were funded in part by MRC grant MR/K015931/1 and BBSRC Alert13 grant BB/L014947/1. RR was funded by the Naseem Manx Brain Tumour Charity. This work is also supported by EPSRC grant EP/N014499/1 "EPSRC Centre for New Mathematical Sciences Capabilities for Healthcare Technologies". We would like to thank Marco Marcello and the Centre for Cell Imaging for provision of training, access to equipment and experimental support.

AUTHOR CONTRIBUTIONS

RR designed the experimental protocols, performed all molecular biology, cell culture and microscopy experiments and analysed the data. DM wrote the code for data processing and implemented the image analysis workflow. DM contributed to image data analysis and interpretation. RB and RL provided help and ideas for mathematical interpretation of the data and for choosing the most relevant output parameters. VS conceived and coordinated the study. RR, DM and VS wrote the manuscript. DM prepared all the figures. All authors reviewed drafts of the manuscript and gave final approval.

COMPETING FINANCIAL INTERESTS

The authors declare no competing interests.

Bibliography

1. S. Walenta, J. Doetsch, W. Mueller-Klieser, and L. A. Kunz-Schughart. Metabolic imaging in multicellular spheroids of oncogene-transfected fibroblasts. *J Histochem Cytochem*, 48 (4):509–22, 2000. ISSN 0022-1554 (Print) 0022-1554 (Linking).
2. Jennifer Laurent, Celine Frongia, Martine Cazales, Odile Mondesert, Bernard Ducommun, and Valerie Lobjois. Multicellular tumor spheroid models to explore cell cycle checkpoints in 3d. *Bmc Cancer*, 13, 2013. ISSN 1471-2407. doi: 10.1186/1471-2407-13-73.
3. Pawel Swietach, Shalini Patiar, Claudiu T. Supuran, Adrian L. Harris, and Richard D. Vaughan-Jones. The role of carbonic anhydrase 9 in regulating extracellular and intracellular ph in three-dimensional tumor cell growths. *Journal of Biological Chemistry*, 284 (30):20299–20310, 2009. ISSN 0021-9258. doi: 10.1074/jbc.M109.006478.
4. D. Hanahan and R. A. Weinberg. The hallmarks of cancer. *Cell*, 100(1):57–70, 2000. ISSN 0092-8674 (Print) 0092-8674 (Linking).
5. Nina Kramer, Angelika Walzl, Christine Unger, Margit Rosner, Georg Krupitza, Markus Hengstschlaeger, and Helmut Dolznig. In vitro cell migration and invasion assays. *Mutation Research-Reviews in Mutation Research*, 752(1):10–24, 2013. ISSN 1383-5742. doi: 10.1016/j.mrrev.2012.08.001.
6. Brendon M. Baker and Christopher S. Chen. Deconstructing the third dimension - how 3d culture microenvironments alter cellular cues. *Journal of Cell Science*, 125(13):3015–3024, 2012. ISSN 0021-9533. doi: 10.1242/jcs.079509.
7. S. Breslin and L. O'Driscoll. Three-dimensional cell culture: the missing link in drug discovery. *Drug Discov Today*, 18(5-6):240–9, 2013. ISSN 1878-5832 (Electronic) 1359-6446 (Linking). doi: 10.1016/j.drudis.2012.10.003.
8. M. Vinci, S. Gowan, F. Boxall, L. Patterson, M. Zimmermann, W. Court, C. Lomas, M. Mendiola, D. Hardisson, and S. A. Eccles. Advances in establishment and analysis of three-dimensional tumor spheroid-based functional assays for target validation and drug evaluation. *Bmc Biology*, 10, 2012. ISSN 1741-7007. doi: Artn2910.1186/1741-7007-10-29.
9. Lin Cheng, Qiulian Wu, Olga A. Guryanova, Zhi Huang, Qian Huang, Jeremy N. Rich, and Shideng Bao. Elevated invasive potential of glioblastoma stem cells. *Biochemical and Biophysical Research Communications*, 406(4), 2011. ISSN 0006-291X. doi: 10.1016/j.bbrc.2011.02.123.
10. Andrew M. Stein, Tim Demuth, David Mobley, Michael Berens, and Leonard M. Sander. A mathematical model of glioblastoma tumor spheroid invasion in a three-dimensional in vitro experiment. *Biophysical Journal*, 92(1):356–365, 2007. ISSN 0006-3495. doi: 10.1529/biophysj.106.093468.
11. S. Blacher, C. Erpicum, B. Lenoir, J. Paupert, G. Moraes, S. Ormenese, E. Bullinger, and A. Noel. Cell invasion in the spheroid sprouting assay: A spatial organisation analysis adaptable to cell behaviour. *Plos One*, 9(5), 2014. ISSN 1932-6203. doi: ARTNe9701910.1371/journal.pone.0097019.
12. E. G. Reynaud, U. Krzic, K. Greger, and E. H. Stelzer. Light sheet-based fluorescence microscopy: more dimensions, more photons, and less photodamage. *HFSP J*, 2(5):266–75, 2008. ISSN 1955-2068 (Print) 1955-205X (Linking). doi: 10.2976/1.2974980.
13. E. H. Stelzer. Light-sheet fluorescence microscopy for quantitative biology. *Nat Methods*, 12 (1):23–6, 2015. ISSN 1548-7105 (Electronic) 1548-7091 (Linking). doi: 10.1038/nmeth.3219.
14. J. Huisken, J. Swoger, F. Del Bene, J. Wittbrodt, and E. H. Stelzer. Optical sectioning deep inside live embryos by selective plane illumination microscopy. *Science*, 305(5686):1007–9, 2004. ISSN 1095-9203 (Electronic) 0036-8075 (Linking). doi: 10.1126/science.1100035.
15. Y. Hou, J. Konen, D. J. Brat, A. I. Marcus, and L. A. D. Cooper. Tasi: A software tool for spatial-temporal quantification of tumor spheroid dynamics. *Sci Rep*, 8(1):7248, 2018. ISSN 2045-2322 (Electronic) 2045-2322 (Linking). doi: 10.1038/s41598-018-25337-4.
16. Kazuhiko Kurozumi, Tomotsugu Ichikawa, Manabu Onishi, Kentaro Fujii, and Isao Date. Cilengitide treatment for malignant glioma: Current status and future direction. *Neurologia Medico-Chirurgica*, 52(8):539–547, 2012. ISSN 0470-8105.
17. Robert H. Kutner, Xian-Yang Zhang, and Jakob Reiser. Production, concentration and titration of pseudotyped hiv-1-based lentiviral vectors. *Nature Protocols*, 4(4):495–505, 2009. ISSN 1754-2189. doi: 10.1038/nprot.2009.22.
18. M. Marcello, R. Richards, D. Mason, and V. See. Live imaging of cell invasion using a multicellular spheroid model and light-sheet microscopy. *Adv Exp Med Biol*, 1035:155–161, 2017. ISSN 0065-2598 (Print) 0065-2598 (Linking). doi: 10.1007/978-3-319-67358-5_11.
19. J. Schindelin, I. Arganda-Carreras, E. Frise, V. Kaynig, M. Longair, T. Pietzsch, S. Preibisch, C. Rueden, S. Saalfeld, B. Schmid, J. Y. Tinevez, D. J. White, V. Hartenstein, K. Eliceiri, P. Tomancak, and A. Cardona. Fiji: an open-source platform for biological-image analysis. *Nat Methods*, 9(7):676–82, 2012. ISSN 1548-7105 (Electronic) 1548-7091 (Linking). doi: 10.1038/nmeth.2019.
20. S. Preibisch, S. Saalfeld, J. Schindelin, and P. Tomancak. Software for bead-based registration of selective plane illumination microscopy data. *Nat Methods*, 7(6):418–9, 2010. ISSN 1548-7105 (Electronic) 1548-7091 (Linking). doi: 10.1038/nmeth0610-418.
21. N. Chenouard, I. Smal, F. de Chaumont, M. Maska, I. F. Sbalzarini, Y. Gong, J. Cardinale, C. Carthel, S. Coraluppi, M. Winter, A. R. Cohen, W. J. Godinez, K. Rohr, Y. Kalaidzidis, L. Liang, J. Duncan, H. Shen, Y. Xu, K. E. Magnusson, J. Jalden, H. M. Blau, P. Paul-Gilloteaux, P. Roudot, C. Kervrann, F. Waharte, J. Y. Tinevez, S. L. Shorte, J. Willemse, K. Celler, G. P. van Wezel, H. W. Dan, Y. S. Tsai, C. Ortiz de Solorzano, J. C. Olivo-Marin, and E. Meijering. Objective comparison of particle tracking methods. *Nat Methods*, 11(3): 281–9, 2014. ISSN 1548-7105 (Electronic) 1548-7091 (Linking). doi: 10.1038/nmeth.2808.
22. J. Y. Tinevez, N. Perry, J. Schindelin, G. M. Hoopes, G. D. Reynolds, E. Laplantine, S. Y. Bednarek, S. L. Shorte, and K. W. Eliceiri. Trackmate: An open and extensible platform for single-particle tracking. *Methods*, 115:80–90, 2017. ISSN 1095-9130 (Electronic) 1046-2023 (Linking). doi: 10.1016/j.ymeth.2016.09.016.
23. M. Vinci, C. Box, M. Zimmermann, and S. A. Eccles. Tumor spheroid-based migration assays for evaluation of therapeutic agents. *Methods Mol Biol*, 986:253–66, 2013. ISSN 1940-6029 (Electronic) 1064-3745 (Linking). doi: 10.1007/978-1-62703-311-4_16.
24. B. Schott, M. Traub, C. Schlagenhauf, M. Takamiya, T. Antritter, A. Bartschat, K. Loffler, D. Blessing, J. C. Otte, A. Y. Kobitski, G. U. Nienhaus, U. Strahle, R. Mikut, and J. Stegmaier. Embryominer: A new framework for interactive knowledge discovery in large-scale cell tracking data of developing embryos. *PLoS Comput Biol*, 14(4):e1006128, 2018. ISSN 1553-7358 (Electronic) 1553-734X (Linking). doi: 10.1371/journal.pcbi.1006128.
25. Shinji Tsutsumi, Kristin Beebe, and Len Neckers. Impact of heat-shock protein 90 on cancer metastasis. *Future Oncology*, 5(5):679–688, 2009. ISSN 1479-6694. doi: 10.2217/fon.09.30.
26. Claire Marie-Elisabeth Sauvageot, Jessica Leigh Weatherbee, Santosh Kesari, Susan Elizabeth Winters, Jessica Barnes, Jamie Dellagatta, Naren Raj Ramakrishna, Charles Dean Stiles, Andrew Li-Jen Kung, Mark W. Kieran, and Patrick Yung Chih Wen. Efficacy of the hsp90 inhibitor 17-aag in human glioma cell lines and tumorigenic glioma stem cells. *Neuro-Oncology*, 11(2):109–121, 2009. ISSN 1522-8517. doi: 10.1215/15228517-2008-060.
27. K. Miekus, J. Kijowski, M. Sekula, and M. Majka. 17aep-ga, an hsp90 antagonist, is a potent inhibitor of glioblastoma cell proliferation, survival, migration and invasion. *Oncol Rep*, 28 (5):1903–9, 2012. ISSN 1791-2431 (Electronic) 1021-335X (Linking). doi: 10.3892/or.2012.1996.
28. O. L. Chinot. Cilengitide in glioblastoma: when did it fail? *Lancet Oncol*, 15(10):1044–5, 2014. ISSN 1474-5488 (Electronic) 1470-2045 (Linking). doi: 10.1016/S1470-2045(14)70403-6.
29. Manabu Onishi, Tomotsugu Ichikawa, Kazuhiko Kurozumi, Kentaro Fujii, Koichi Yoshida, Satoshi Inoue, Hiroyuki Michiue, E. Antonio Chiocca, Balveen Kaur, and Isao Date. Bimodal anti-glioma mechanisms of cilengitide demonstrated by novel invasive glioma models. *Neuropathology*, 33(2):162–174, 2013. ISSN 0919-6544. doi: 10.1111/j.1440-1789.2012.01344.x.
30. A. Wilisch-Neumann, N. Kliese, D. Pachow, T. Schneider, J. P. Warnke, W. E. Braunsdorf, F. D. Bohmer, P. Hass, D. Pasemann, C. Helbing, E. Kirches, and C. Mawrin. The integrin inhibitor cilengitide affects meningioma cell motility and invasion. *Clin Cancer Res*, 19(19): 5402–12, 2013. ISSN 1078-0432 (Print) 1078-0432 (Linking). doi: 10.1158/1078-0432.CCR-12-0299.
31. G. D. Maurer, I. Tritschler, B. Adams, G. Tabatabai, W. Wick, R. Stupp, and M. Weller. Cilengitide modulates attachment and viability of human glioma cells, but not sensitivity to

PREPRINT

irradiation or temozolomide in vitro. *Neuro Oncol*, 11(6):747–56, 2009. ISSN 1523-5866. doi: 10.1215/15228517-2009-012.

32. P. G. Gritsenko and P. Friedl. Adaptive adhesion systems mediate glioma cell invasion in complex environments. *Journal of Cell Science*, 131(15), 2018. ISSN 0021-9533. doi: UNSPjcs21638210.1242/jcs.216382.
33. A. Farin, S. O. Suzuki, M. Weiker, J. E. Goldman, J. N. Ruce, and P. Canoll. Transplanted glioma cells migrate and proliferate on host brain vasculature: A dynamic analysis. *Glia*, 53 (8):799–808, 2006. ISSN 0894-1491. doi: 10.1002/glia.20334.
34. R. H. Goldbrunner, H. K. Haugland, C. E. Klein, S. Kerkau, K. Roosen, and J. C. Tonn. Ecm dependent and integrin mediated tumor cell migration of human glioma and melanoma cell lines under serum-free conditions. *Anticancer Research*, 16(6B):3679–3687, 1996. ISSN 0250-7005.
35. Marisol Herrera-Perez, Sherry L. Voytik-Harbin, and Jenna L. Rickus. Extracellular matrix properties regulate the migratory response of glioblastoma stem cells in three-dimensional culture. *Tissue Engineering Part A*, 21(19-20):2572–2582, 2015. ISSN 1937-3341. doi: 10.1089/ten.tea.2014.0504.
36. K. Wolf, M. te Lindert, M. Krause, S. Alexander, J. te Riet, A. L. Willis, R. M. Hoffman, C. G. Figdor, S. J. Weiss, and P. Friedl. Physical limits of cell migration: Control by ecm space and nuclear deformation and tuning by proteolysis and traction force. *Journal of Cell Biology*, 201(7):1069–1084, 2013. ISSN 0021-9525. doi: 10.1083/jcb.201210152.
37. Muhammad H. Zaman, Linda M. Trapani, Alisha Siemeski, Drew MacKellar, Haiyan Gong, Roger D. Kamm, Alan Wells, Douglas A. Lauffenburger, and Paul Matsudaira. Migration of tumor cells in 3d matrices is governed by matrix stiffness along with cell-matrix adhesion and proteolysis. *Proceedings of the National Academy of Sciences of the United States of America*, 103(29):10889–10894, 2006. ISSN 0027-8424. doi: 10.1073/pnas.0604460103.
38. W. B. Pratt and D. O. Toft. Regulation of signaling protein function and trafficking by the hsp90/hsp70-based chaperone machinery. *Experimental Biology and Medicine*, 228(2): 111–133, 2003. ISSN 1535-3702.
39. A. Taiyab and M. Rao Ch. Hsp90 modulates actin dynamics: inhibition of hsp90 leads to decreased cell motility and impairs invasion. *Biochim Biophys Acta*, 1813(1):213–21, 2011. ISSN 0006-3002 (Print) 0006-3002 (Linking). doi: 10.1016/j.bbamcr.2010.09.012.
40. P. Leblond, A. Dewitte, F. Le Tinier, C. Bal-Mahieu, M. Baroncini, T. Sarrazin, E. Lartigau, A. Lansiaux, and S. Meignan. Cilengitide targets pediatric glioma and neuroblastoma cells through cell detachment and anoikis induction. *Anticancer Drugs*, 24(8):818–25, 2013. ISSN 1473-5741. doi: 10.1097/CAD.0b013e328362edc5.

PREPRINT

Supplementary Data

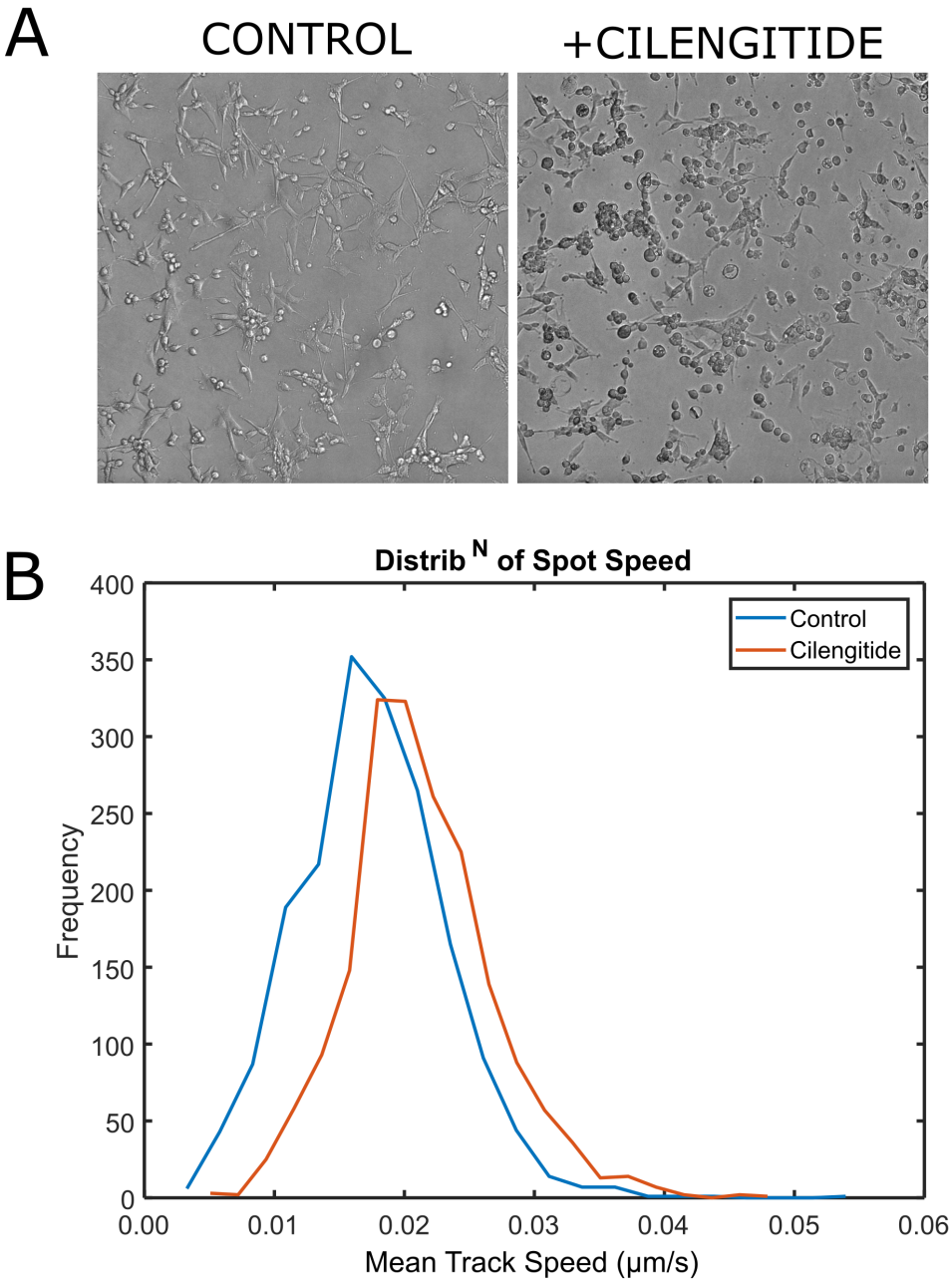

Figure S1. (A) Cilengitide treatment in 2D culture. U87MG glioblastoma cells grown in 2D cell culture show a more rounded, less adhesive phenotype when pre-treated with cilengitide. (B) When tracked over 16 hours, cilengitide-treated cells show a slightly faster track speed.

Supplementary Data

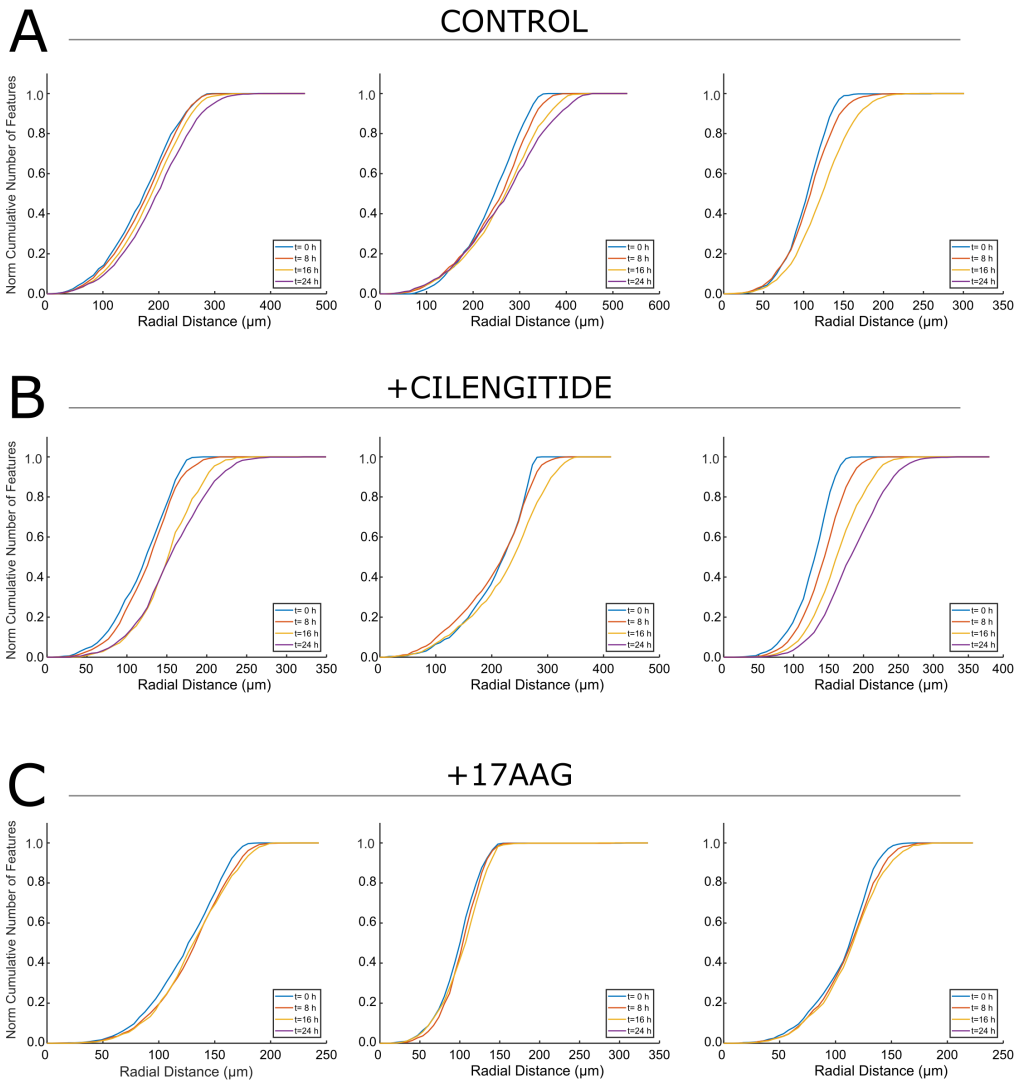

Figure S2. The cumulative distribution of cells (as a function of distance from the spheroid centroid) is shown for three replicates of control (A), cilengitide-treated (B) and 17AAG-treated (C) spheroids over time.

Supplementary Movies

Supplementary Movie 1. Invasion into the matrix. Glioblastoma spheroids made up of U87 cells expressing H2B-RFP were grown for 3 days, mounted on a lightsheet microscope (0 h) and imaged for up to 24 h. The movie is rendered using Imaris.

Supplementary Movie 2. Cilengitide treatment does not affect invasion. Glioblastoma spheroids made up of U87 cells expressing H2B-RFP were grown for 3 days, mounted on a lightsheet microscope with 2 μM cilengitide (0 h) and imaged for up to 24 h. The movie shows a maximum intensity projection through the z-plane.

Supplementary Movie 3. 17AAG treatment affect both migration and invasion. Glioblastoma spheroids made up of U87 cells expressing H2B-RFP were grown for 3 days, mounted on a lightsheet microscope with 0.5 μM 17AAG (0 h) and imaged for up to 24 h. The movie shows a maximum intensity projection through the z-plane.

PREPRINT